Mixed-phase MOF-derived Titanium Dioxide for Photocatalytic Hydrogen Evolution: The Impact of the Templated Morphology

Stavroula Kampouri[a]†, Christopher P. Ireland[a]†, Bardiya Valizadeh[a], Emad Oveisi[b], Pascal A. Schouwink[c], Mounir Mensi[c] and Kyriakos C. Stylianou[a]*

[a] Laboratory of Molecular Simulation (LMSO), Institute of Chemical Sciences and Engineering, École Polytechnique Fédérale de Lausanne (EPFL Valais), Rue de l'industrie 17, 1951 Sion, Switzerland,

[b] Interdisciplinary Center for Electron Microscopy, École Polytechnique Fédérale de Lausanne (EPFL), CH-1015 Lausanne, Switzerland,

[c] Institute of Chemical Sciences and Engineering, École Polytechnique Fédérale de Lausanne (EPFL Valais), Rue de l'industrie 17, 1951 Sion, Switzerland

ABSTRACT:

Herein, we explored a simple metal-organic framework (MOF) mediated synthesis for the controlled preparation of pure and mixed phase titania (TiO_2) nanoparticles. Scanning electron microscopy images revealed that the MOF-derived TiO_2 retain the MOF crystal shape, and through powder X-ray diffraction and X-ray photoelectron spectroscopy, it is demonstrated that the crystal-template is composed of nanosized TiO_2 rutile and anatase particles. The presence of both TiO_2 rutile and anatase phases in the crystal-template enhances the interactions between them, thus suppressing the electron-hole recombination. This has an impact toward the photocatalytic reduction of water as the templated MOF-derived TiO_2 outperforms the commercial (P25 Degussa), titanium isopropoxide-derived and non-templated MOF-derived TiO_2. Our study demonstrates that the morphologically-induced high charge separation efficiency afforded by using MOF crystals as precursors can lead to the generation of catalytically more active materials that can challenge existing photocatalysts in the field of hydrogen generation.

KEYWORDS: *photocatalysis, hydrogen evolution, MIL-125-NH₂, TiO₂, templated morphology, MOF-mediated synthesis*

INTRODUCTION

The atmospheric pollution induced by the combustion of fossil fuels, along with the continuously growing energy demand have prompted intense research in the employment of hydrogen (H_2), as an environmentally friendly energy carrier. Among other ways, such as steam methane reformation or coil gasification, photocatalytic water splitting is a sustainable approach to produce H_2 by harnessing light energy, which can be provided by the inexhaustible sun.[1] Titanium dioxide (TiO_2) was the first material investigated for the photocatalytic splitting of water[2-4] and is still considered among the most promising photocatalysts, due to its chemical and thermal stability, non-toxicity, high reactivity and low cost.[5-7] Despite the fact that tremendous research efforts have been focused on the use of TiO_2 nanoparticles (NPs) in a variety of photocatalytic applications (water splitting, water remediation, CO_2 reduction),[8] the impact of the shape and morphology of TiO_2 NPs as well as the interplay between the two most common phases of TiO_2 (rutile and anatase) remain questionable.

The low temperature TiO_2 anatase phase is generally recognized as a better catalyst towards the H_2 evolution reaction, due to the surface hydration, meaning that a higher concentration of active sites is present compared with the TiO_2 rutile phase. Nevertheless, the more thermodynamically stable TiO_2 rutile phase has a smaller band gap implying that a significant higher proportion of light can be absorbed, thus careful engineering of a single TiO_2 rutile phase particles can lead to enhanced photocatalytic performance.[9] On the other hand, materials based on mixed TiO_2 rutile and anatase phases have demonstrated superior photocatalytic performance in comparison with the single phase TiO_2.[10-14] P25 Degussa, a mixed phase commercial TiO_2 is widely used as a standard material for photocatalysis and was studied by Bickley in 1990 to ascertain its success compared to a single phase TiO_2.[10] The conclusion was that the excellent electronic contact between the two phases allowed successful electron-hole separation.

Subsequent literature has both agreed[11-12] and disputed[13] these findings and specifically the morphology of the phases' interface and the interactions between them. However, ample evidence has been provided through both experimental and computational approaches to prove that there is indeed a synergy between the anatase and rutile phases, allowing more efficient electron-hole separation.[14] A general understanding has therefore been developed that TiO_2 materials with the anatase and rutile phases in a 3:1 ratio can outperform comparably formed single phase TiO_2. The different structural arrangement of TiO_2 anatase and rutile phases affords distinct phase electronic structures. As conclusively demonstrated by Scanlon et al.,[15] close electronic contact between the two phases allows electrons on rutile TiO_2 to irreversibly transfer to the complementary TiO_2 anatase phase, with this synergy promoting the electron-hole separation.

In order to engineer this electronic contact between the two TiO_2 phases, several synthetic techniques have been utilized; approaches of physically mixing anatase and rutile TiO_2 have been attempted, but mixing does not allow the two phases to sufficiently interact with each other and achieve this synergy.[16-17] Synthetic efforts on mixed phase TiO_2 have employed the sol-gel route, hydro/solvo-thermal method, electrodeposition, direct oxidation method or chemical vapor deposition.[18] Many of these techniques, however lack of control, are impractical or may not provide highly active and stable TiO_2 NPs.

Metal-organic frameworks (MOFs) are crystalline materials that consist of metal ions or clusters coordinated to organic ligands to form 3-dimensional porous structures. Due to their high crystallinity, structural tuneability and porous nature, MOFs have been extensively explored for a variety of applications.[19-20] Whilst, MOFs themselves have high potential, limitations related to their thermal and chemical stability have recently triggered their utilization as precursors for the preparation of highly stable metal oxides with catalytic activities.[21-26] More specifically, the MOF-mediated synthesis involves the use of MOFs as crystalline self-sacrificing templates in order to tailor the shape, composition, surface area and stability of the resulting materials.[27-28] Calcination of MOFs in air leads to the partial or complete burning of the organic ligands and formation of highly active metal-oxide NPs, while carbonization at high temperature under inert conditions can result in a carbon matrix encapsulating the metal phase (NPs) and thus avoiding sintering effects.[29]

Among the Ti^{IV}-based MOFs, the MIL-125 series consisting of functionalized (or not) ligands exhibit a 3-dimensional and porous structure, and represent the most studied Ti^{IV}-based MOFs for photocatalytic applications.[30-32] Recently, MIL-125-NH_2 was utilized as a precursor for the synthesis TiO_2 particles, decorated with either palladium or gold NPs for photocatalytic applications, such as CO_2 reduction and hydrogen evolution.[33-34] The employment of expensive noble metal NPs as co-catalysts was necessary to enhance the

otherwise inadequate photocatalytic performance of TiO_2, due to high electron-hole recombination rates. Although these studies provided important insights, there is still a need to better understand the impact of templated MOF-derived TiO_2 rutile and anatase phases, and the effect of the morphology on the synergy between the two phases in photocatalysis.

Herein, we investigate primarily the photocatalytic performance of TiO_2 prepared using the MIL-125-NH$_2$ as a starting material. By calcining MIL-125-NH$_2$ over a range of temperatures, the ratio of the anatase and rutile phases could be controlled. The resulting TiO_2 retained the well-defined crystal shape of the parent MOF upon heating. The best performing mixed TiO_2 anatase-rutile phase (ratio 66:34) exhibits a H_2 evolution rate of 1394 $\mu mol\ h^{-1}\ g^{-1}$. For comparison, MIL-167-derived TiO_2, and TiO_2 synthesized from precipitated amorphous titanium hydroxide were prepared, all of which demonstrated inferior photocatalytic performances. Morphological studies revealed the unique nature of the templated MIL-125-NH$_2$-derived TiO_2 with nanosized anatase and rutile NPs forced into effective contact with each other, leading to an efficient electron-hole separation. In addition, the templated MIL-125-NH$_2$-derived mixed phase TiO_2 outperforms the commercial Degussa P25 TiO_2. Our work highlights the role of effective interactions of TiO_2 anatase and rutile phases in a template, and offers an intriguing outline for the development of efficient photocatalysts.

RESULTS AND DISCUSSION

MIL-125-NH$_2$ was synthesized based on a reported procedure (see section S1.2)[35] and its phase purity was confirmed by powder X-ray diffraction (PXRD) (Figure S1). Prior to the MOF-mediated synthesis of TiO_2, the thermogravimetric analysis (TGA) of MIL-125-NH$_2$ was carried out. Figure 1a shows the TGA profile of MIL-125-NH$_2$. Two major weight losses are observed; from 30 to ~200 °C, owed to the removal of guest molecules from the pores of the MIL-125-NH$_2$ and from 360 to 600 °C related to the structural collapse of MIL-125-NH$_2$. The final product obtained after heating MIL-125-NH$_2$ at 600 °C corresponds to the remaining metal oxide, TiO_2, as confirmed by PXRD.

Acquiring a clear perception regarding the thermally-induced structural collapse of the MIL-125-NH$_2$, allowed us to continue with the synthesis of MOF-derived TiO_2 at selected temperatures (400 - 800 °C) under air (see section S1.2, Figure 1b). As can be seen in Figure 1c, calcination at different temperatures yields TiO_2 with differing ratios of the TiO_2 anatase and rutile phases. The anatase to rutile transformation is reconstructive, meaning that it involves the breaking of chemical bonds. The transformation temperature itself can vary depending on the starting material particle size, shape and volume and experimental factors such as atmosphere, heating rate and sample container. Reported temperatures for the TiO_2 anatase to rutile transformation vary from 400 to 1200°C.[36]

Presently, heating the MIL-125-NH$_2$ crystals up to 400 °C leads to the formation of pure TiO_2 anatase phase. Increasing the temperature to 500°C induces the formation of the rutile phase (giving rise to a mixed phase TiO_2), which gradually becomes the dominant phase at 800 °C. Here, the anatase to rutile phase transformation is at the lower end of the temperature range reported for this transformation.[37] [38]

Further insights into the specific crystallization process can be gained from a variable temperature (VT) PXRD experiment, where MIL-125-NH$_2$ enclosed in a quartz capillary was heated from 30 to 800 °C (see section S1.3, Figure S2, Figure S3). Although direct comparison of ex-situ and in-situ experiments is not applicable (due to the crystallization process being rather complex and related to heating rate, dwell time and volume of the heating

vessel), the in-situ VT PXRD experiment offers an insight into the TiO_2 anatase and rutile phase formation. Upon heating, the PXRD patterns show that the Bragg reflections of MIL-125-NH_2 are eliminated due to decomposition, leading to an amorphous powder. Upon further heating, initial formation of the TiO_2 anatase phase is observed as a broad hump at 25.2 ° 2θ (Figure S2), at furnace temperature of 560 °C. The peak width (Full width half maximum: FWHM 1.73 2θ) manifests a lack of crystallinity which can be indicative of defects and a small domain size. This poor crystallinity may be related to the removal of the organic ligand which disrupts the crystallization process at the initial stages of TiO_2 formation. Interestingly, further heating to 660°C revealed the formation of a more crystalline TiO_2 rutile phase with a FWHM of 0.31 2θ. The integral intensity of the TiO_2 anatase Bragg peak remains constant during initial rutile formation, suggesting that the initial formation results from the same matrix as anatase. Both phases co-exist before the TiO_2 rutile phase becomes the dominant phase at 785 °C. The TiO_2 anatase and rutile phase composition, and the average domain size were quantified by Rietveld refinement from the as-prepared TiO_2 samples (Table 1). It is found that the domain size for both TiO_2 anatase and rutile phases is comparable at the same temperature, and increases with temperature.

To serve as a reference, different pure and mixed phase TiO_2 were also obtained by calcining (400 - 800 °C) precipitated amorphous titanium hydroxide (TiH_4O_4) as a starting material (see section S1.2). The TGA profile of the TiH_4O_4 shows a weight loss up to 450 °C, related to the removal of hydroxide, coordinated water and/or organic residues derived from the titanium isopropoxide (Figure S4). Upon calcination, the TiO_2 anatase to rutile phase transformation starts at 700 °C and above this temperature, the TiO_2 rutile phase becomes dominant (Figure 1d). VT PXRD experiments collected on TiH_4O_4, using the same protocol used with MIL-125-NH_2 revealed that the formation of TiO_2 anatase phase begins at a significantly lower temperature than the MIL-125-NH_2-derived TiO_2, with peaks of anatase identified as low as 180°C (Figure S5, Figure S6). Interestingly, the qualitative trend of domain-sizes of anatase and rutile is inversed between MIL-125-NH_2 and TiH_4O_4-derived samples, with initial rutile formation from TiH_4O_4 showing a much larger FWHM than from MIL-125-NH_2. This suggests that nucleation and growth proceeds through different mechanisms, which is likely related to the topological differences between a pre-existing framework/matrix of Ti-O polyhedral in TiH_4O_4 as opposed to discrete Ti-O clusters separated by the organic ligands in MIL-125-NH_2. Furthermore, the ex-situ determined domain size of the TiO_2 anatase phase is significantly greater than that of the MIL-125-NH_2-derived material, with the FWHM only 0.73 2θ, implying a much higher degree of crystallinity. This improved crystallinity delays the formation of the rutile phase to 710 °C. [36]

X-ray photoelectron spectroscopy (XPS) were performed, to analyze the surface of the mixed phase material. XPS revealed a titanium 2p peak at a binding energy of 458.5 eV. Each TiO_2 rutile and anatase phase has a distinct binding energy separated by 0.4 eV, allowing us to quantify the composition of both phases on the surface of TiO_2.[15] From the fitting, the TiO_2 anatase and rutile phase composition of the MIL-125-NH_2-derived TiO_2 at 600 ° C is 15:85 (Figure S7a) indicating a higher rutile content on the surface compared to the bulk (66:34). This higher surface rutile content is also the case with the TiH_4O_4-derived TiO_2 (Figure S7b). This analysis is consistent with the thermal heating process involved, whereby the surface of the particle is where the initial transformation between anatase and rutile takes place.
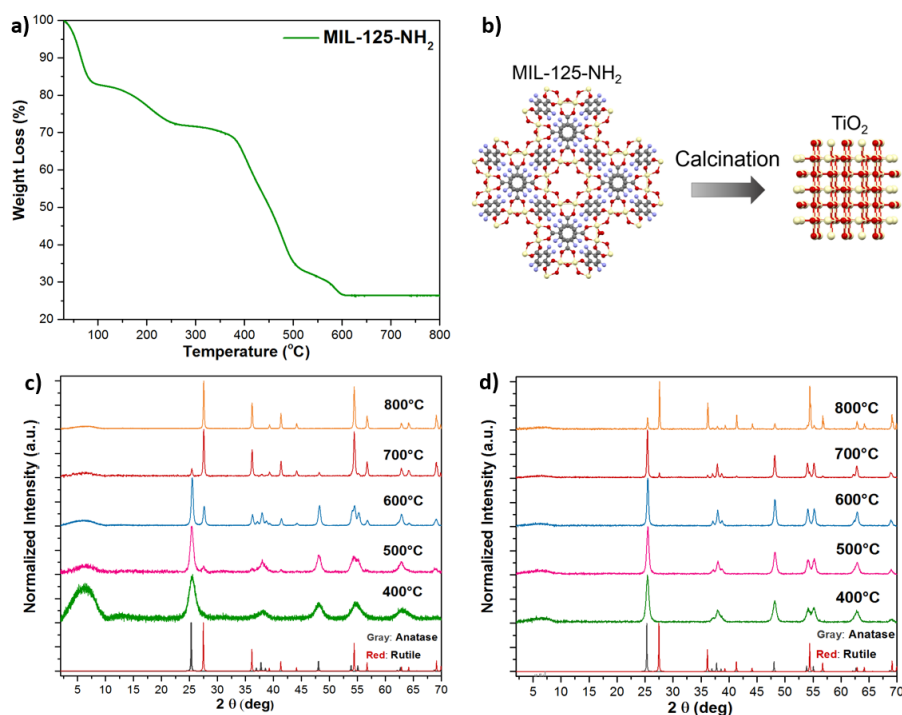
Figure 1. a) TGA curve of MIL-125-NH$_2$ obtained under airflow with a heating rate of 5 °C min^{-1}. b) Schematic illustration of the synthetic procedure of MIL-125-NH$_2$-derived TiO$_2$. PXRD patterns of the as-synthesized c) MIL-125-NH$_2$-derived and d) TiH$_4$O$_4$-derived TiO$_2$.

Figure S8 displays the Kubelka-Munk representation of the UV-vis diffuse reflectance spectra of TiO$_2$ synthesized from MIL-125-NH$_2$ and TiH$_4$O$_4$. The spectra of both families are in agreement with the literature,[39] with the presence of rutile, which has a smaller band gap, causing a red shift in the light absorption edge compared to phase pure anatase TiO$_2$. In the case of the MIL-125-NH$_2$-derived TiO$_2$ synthesized through calcination at 400 °C, there is an extended light absorbance in the visible region, which is attributed to the residual carbon from the MIL-125-NH$_2$ covering the surface of TiO$_2$ and is in agreement with the TGA data (Figure 1a).

Table 1. PXRD-derived data revealing the size and composition of TiO$_2$ synthesized using MIL-125-NH$_2$ and TiH$_4$O$_4$ as precursors.

	MIL-125-NH$_2$-derived TiO$_2$					TiH$_4$O$_4$-derived TiO$_2$				
Synthesis Temp. (°C)	400	500	600	700	800	400	500	600	700	800
Anatase (w.t. %)	98	87	66	11	-	100	100	100	92	20
Rutile (w.t. %)	2	13	34	89	100	-	-	-	8	80
Size Anatase (nm)	5.7	11	22	44	-	13	17	26	43	56
Size Rutile (nm)	5.9	12	25	47	61	-	-	-	87	87

The morphologies of MIL-125-NH$_2$- and TiH$_4$O$_4$-derived TiO$_2$ were investigated through scanning electron microscopy (SEM) (see section S2.7). As can be seen in Figure 2, the well-defined crystal shape of MIL-125-

NH$_2$ is retained during heating. It is found that the MIL-125-NH$_2$-derived TiO$_2$ exhibits a rectangular parallelepiped with round corners shape and its size is significantly reduced compared to the 1 μm MIL-125-NH$_2$-crystals (Figure 2a). The size reduction is associated with the high calcination temperature and subsequently to the removal of the guest-molecules and organic ligand in MIL-125-NH$_2$. Transmission electron microscopy (TEM) images show that the crystal-templates consisted of nanosized TiO$_2$ NPs (Figure 3a,b, S9 and S10). This is further confirmed by dark-field TEM, where the incident electron beam is tilted so that only the reflections of specific diffracting crystallographic planes contribute to image formation (Figure S9 and S10). Depending on the diffraction angle, TiO$_2$ NPs of specific crystallographic orientation are illuminated in the dark-field image, confirming the multi-particle nature of the crystal-template. The co-existence of both TiO$_2$ rutile and anatase phases produced at 600 °C was additionally proven by selected area electron diffraction (SAED) pattern measurements (Figure 3c). The observed diffraction pattern is comparable with Bikley's seminal work on P25, with the many nanosized TiO$_2$ particles diffracting to give Debye-Scherrer rings.[10] These rings can be indexed to both TiO$_2$ anatase and rutile phases, confirming the multiphase nature of this material (Figure 3c).

In contrast to the MIL-125-NH$_2$-derived TiO$_2$, the morphology of TiH$_4$O$_4$-derived TiO$_2$ resembles disordered arrangement of bulk aggregates (Figure S11, S12 and S13), typical of precipitated and co-precipitated metal oxide NPs, and indeed reminiscent of P25 TiO$_2$ NPs.[40] The differing morphology of the MIL-125-NH$_2$- and TiH$_4$O$_4$-derived TiO$_2$ offer up an intriguing question of how this could affect the synergy between the TiO$_2$ anatase and rutile phases.
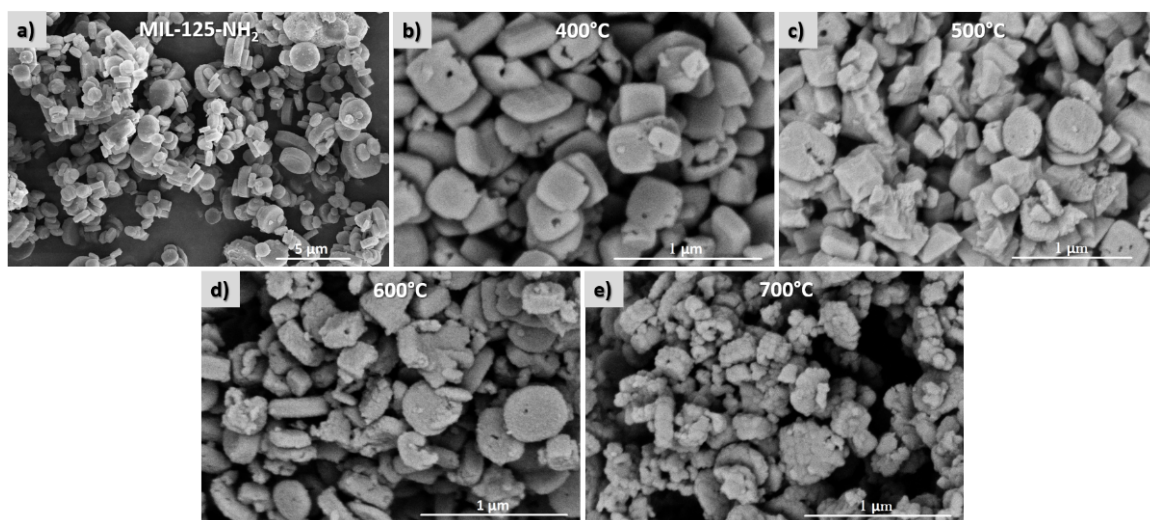

Figure 2. SEM image of a) MIL-125-NH$_2$ and MIL-125-NH$_2$-derived TiO$_2$ samples synthesized at b) 400 °C, c) 500 °C, d) 600 °C and e) 700 °C for 1 h. The images are of the same magnification except for MIL-125-NH$_2$, which is of 5 times less magnification in order to display the morphology of the larger MOF crystals.
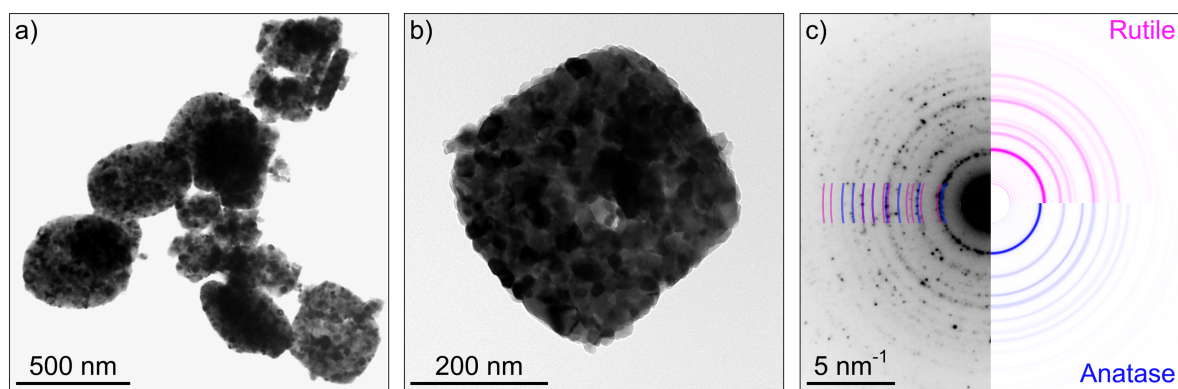
Figure 3. a,b) Bright-field TEM images and c) selected area electron diffraction pattern of MIL-125-NH$_2$-derived TiO$_2$ synthesized through calcination at 600°C for 1 h. Simulated electron diffraction patterns of anatase and rutile phases (ring sampling diffraction planes) are shown to the right of the image for reference.

After characterization, the performance of the MIL-125-NH$_2$-derived TiO$_2$ NPs was investigated toward the photocatalytic H$_2$ evolution from water, with methanol used as the sacrificial electron donor (20 v/v%) in the absence of co-catalyst, under UV-Vis light radiation, from a 300 W Xe lamp (see section S3). As shown in Figure 4a, the ratio between the TiO$_2$ anatase and rutile phases was found to have a profound impact on the photocatalytic performance. More specifically, increasing the rutile phases induces a volcano type trend with respect to the H$_2$ evolution rate. The sample with a composition of 66 w.t.% TiO$_2$ anatase and 34 w.t.% TiO$_2$ rutile (synthesized through calcination of MIL-125-NH$_2$ at 600°C) exhibits the highest H$_2$ evolution rate of 1394 μmol h^{-1} g^{-1}. Materials with higher amounts of TiO$_2$ rutile phase deteriorate their photocatalytic performance and the H$_2$ evolution rate for the TiO$_2$ with composition of 11 w.t.% TiO$_2$ anatase, 89 w.t.% TiO$_2$ rutile is 372 μmol h^{-1} g^{-1}. The same trend between the activity and the ratio between the TiO$_2$ anatase and rutile phases was observed for the TiH$_4$O$_4$-derived TiO$_2$, with the 92 w.t% anatase and 8 w.t.% rutile TiO$_2$ exhibiting the best photocatalytic performance, with a H$_2$ evolution rate of 259 μmol h^{-1} g^{-1} (Figure 4b).

The higher photoactivity of the mixed-phase TiO$_2$ (66 w.t.% TiO$_2$ anatase and 34 w.t.% TiO$_2$ rutile), as compared to the phase pure TiO$_2$ anatase or rutile, is thought to be owed to the synergistic effect between the two polymorphs. This allows for a more efficient charge carrier separation, provided that the two phases are in good electronic contact. The photogenerated electrons flow from the TiO$_2$ rutile to the TiO$_2$ anatase phase, which finally catalyzes the H$_2$ evolution reaction.[15] Recycling experiments were carried out for the best performing TiO$_2$ for three consecutive cycles. The photostability and the morphology of the MIL-125-NH$_2$-derived TiO$_2$ were fully preserved, with consistent H$_2$ rates produced over 3 cycles (Figure S14a). The SEM images of TiO$_2$ after photocatalysis demonstrated that the templated morphology of the material was conserved, and PXRD showed no loss of crystallinity with the same TiO$_2$ anatase-rutile phase composition (Figure S14b and c).
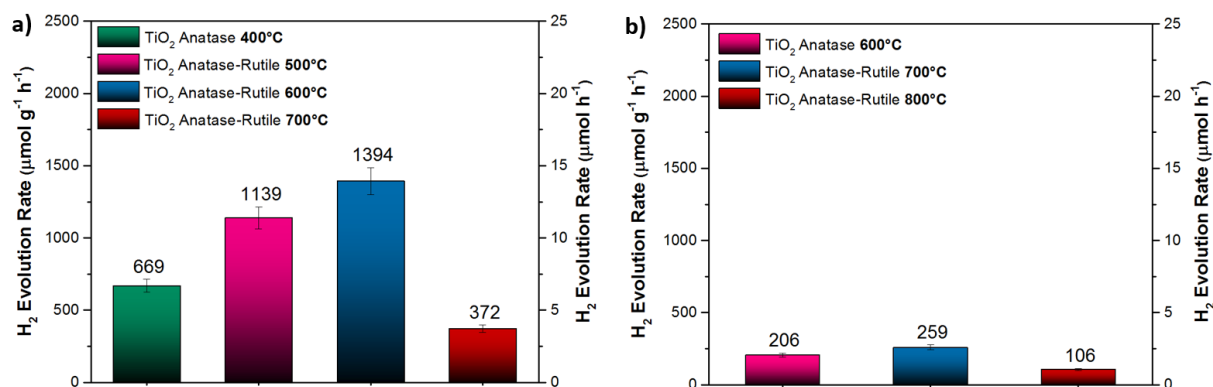
Figure 4. Comparison of H_2 evolution rates of a) MIL-125-NH_2-derived TiO_2 samples synthesized at different temperatures and b) TiH_4O_4-derived TiO_2 samples synthesized at 600°C (anatase), 700°C (anatase-rutile) and 800°C (anatase-rutile).

Intrigued by these results, the photocatalytic performance of two additional TiO_2 samples consisting of both the TiO_2 anatase and rutile phases was explored; the commercial P25 Degussa TiO_2 (with anatase-rutile phases in a composition of approximately 70 : 30)[40] and another MOF-derived TiO_2 using MIL-167 as the precursor.[41] Figure S15 demonstrates the successful synthesis of MIL-167-derived TiO_2 NPs by calcination of the precursor at 600 °C for 1 h in air (See section S1.2). Under these conditions, a mixed phase TiO_2 with composition of TiO_2 75 w.t.% anatase and 25 w.t.% rutile was prepared (Table S1). SEM images (Figure S16) show that the morphology of MIL-167-derived TiO_2 is based upon irregularly shaped aggregates with a large size of 5-20 μm. Despite the use of crystalline MOF as precursor, the morphology of MIL-167-derived TiO_2 is more comparable with the TiH_4O_4-derived TiO_2 than the MIL-125-NH_2 derived TiO_2. TEM images indicate that the size of the MIL-167-derived TiO_2 NPs is 30-40 nm, which is significantly larger than that of the TiO_2 NPs derived from MIL-125-NH_2 (Figure S17).

The photocatalytic performance of the different mixed phase TiO_2 is shown in Figure 5a. The best MIL-125-NH_2-derived TiO_2 outperforms all the other TiO_2 samples, including the commercially available P25 Degussa.[10] This is despite the relatively higher BET surface area of P25 Degussa compared to the other TiO_2 samples (Figure S18). More specifically, the P25 Degussa TiO_2 exhibited a H_2 evolution rate of 624 μmol h^{-1} g^{-1}, followed by the MIL-167-derived sample with a rate of 274 μmol h^{-1} g^{-1}, which is comparable to that achieved by the TiH_4O_4-derived TiO_2 (259 μmol h^{-1} g^{-1}). For the best performing MIL-125-NH_2-derived TiO_2 and P25 Degussa, the dependence of the H_2 evolution rate on the concentration of photocatalyst in solution was further explored and found that the MIL-125-NH_2-derived TiO_2 reaches a higher plateau than that of the P25 Degussa TiO_2 (Figure S19). This implies that the required amount of MIL-125-NH_2-derived TiO_2 photocatalyst is lower, indicative of a well dispersed sample in solution.[42] The Kubelka-Munk representation of the UV-vis diffuse reflectance spectra of the examined samples is illustrated in Figure S20. The indirect band gap for each of the materials was extrapolated from the linear section of the Tauc plot for an indirect bandgap. It can be seen that the indirect band gap is similar for all samples; 2.96 eV for MIL-125-NH_2-derived and MIL-167-derived TiO_2, 2.98 eV for TiH_4O_4-derived and 3.08 eV for P25 Degussa.
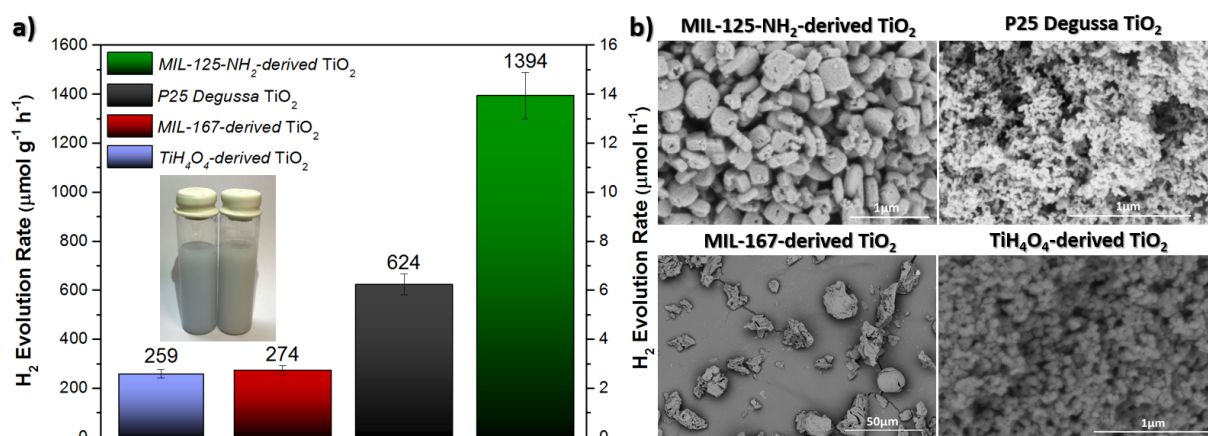
Figure 5. a) Comparison of photocatalytic activity and b) SEM images of the MIL-125-NH$_2$-, MIL-167-, TiH$_4$O$_4$-derived TiO$_2$ and P25 Degussa. Inset: Photograph of the light-blue-colored P25 Degussa (left) and the MIL-125-NH$_2$-derived TiO$_2$ (right), after the photocatalytic test.

The superior photocatalytic performance of the MIL-125-NH$_2$-derived TiO$_2$ NPs over the other TiO$_2$ samples can be attributed to the morphology differences observed in SEM and TEM images (Figure 5b). The fact that the precursors in MOF-mediated syntheses are themselves well-defined crystals allows the resulting templated TiO$_2$ NPs to retain an exceptional close contact throughout the calcination and transformation process. These findings highlight that the TiO$_2$ anatase to rutile phase ratio is not the only predominant factor determining the photocatalytic performance, since excellent electronic contact between the two TiO$_2$ phases is a prerequisite for successful electron-hole separation and thus high photocatalytic activity.

Furthermore, it was observed from the photocatalysis experiments that the MIL-125-NH$_2$-derived TiO$_2$ suspension retained its white color throughout the photocatalytic test, in contrast to TiO$_4$H$_4$-, MIL-167-derived TiO$_2$ and P25, which obtained a blue hue (Inset at Figure 5a). The blue color is attributed to the presence of Ti^{III} in the TiO$_2$, indicative of inefficient electron transport from the TiO$_2$ NPs to the water molecules or protons. Nevertheless, in the case of the MIL-125-NH$_2$-derived TiO$_2$, there was no Ti^{III} observed, indicating superior electron transport and water reduction.

To further study this, photoluminescence (PL) experiments were performed to follow the irradiative recombination of the photo-excited charge carriers in the different TiO$_2$ samples and thus to gain further insights into the charge separation efficiency (Figure S21). In principle, the electron-hole recombination can occur through different pathways, including irradiative recombination through trap states, in addition to the irradiative band gap emission, which is less observed with TiO$_2$, being an indirect band gap semiconductor.[43] In order to facilitate the comparison, the irradiative recombination of photogenerated charge carriers was quantified by integrating the PL emission curves of the different TiO$_2$ samples (Table S2). The PL emission followed the order: MIL-167-derived TiO$_2$ > TiH$_4$O$_4$-derived TiO$_2$ > P25 Degussa > MIL-125-NH$_2$-derived TiO$_2$. The PL results exhibit a comparable trend with the photocatalytic results, as the MIL-125-NH$_2$-derived TiO$_2$, which photocatalytically outperformed the other TiO$_2$ samples demonstrated the lowest PL emission, followed by the P25, which was the second best performing photocatalyst.

CONCLUSIONS

In summary, we report a synthetic method in which MIL-125-NH$_2$ crystals were used as a precursor for the preparation of TiO$_2$ NPs composed of pure or mixed rutile and anatase phases. The crystals of MIL-125-NH$_2$ act as a template for the synthesis of TiO$_2$ and the templated mixed-phase TiO$_2$ (with anatase to rutile composition of 66:34) produced a H$_2$ rate of 1394 μmol h^{-1} g^{-1}. The optimum MIL-125-NH$_2$-derived TiO$_2$ notably outperformed the commercial P25 Degussa, the conventionally synthesized TiH$_4$O$_4$- and MIL-167-derived TiO$_2$. Two major aspects explain the high photocatalytic activity of the MIL-125-NH$_2$-derived TiO$_2$: *i.* the unique morphology that facilitates the constrained contact of NPs between the TiO$_2$ anatase and rutile phases and *ii.* the distribution of the TiO$_2$ anatase and rutile phases within the MIL-125-NH$_2$-derived template. These combine to result in an enhanced synergistic effect, which significantly suppresses the undesired electron-hole recombination. Our study highlights that high charge separation efficiency can be morphologically-induced within TiO$_2$ by using crystalline starting materials.

ASSOSIATED CONTENT

Supporting Information

The Supporting Information is available free of charge on the ACS Publication website at DOI: xx.

Experimental methods, materials, synthetic procedures, PXRD, TGA, Elemental analyses, SEM and TEM images, XPS, N$_2$ isotherms and photocatalytic experiments are shown in the Supporting Information.

AUTHOR INFORMATION

Corresponding Author

* Email: kyriakos.stylianou@epfl.ch

Notes

† Denotes equal contribution to authorship

The authors declare no competing financial interest.

ACKNOWLEDGEMENTS

REFERENCES

(1) Zou, X.; Zhang, Y. Noble Metal-free Hydrogen Evolution Catalysts for Water Splitting. *Chem. Soc. Rev.* **2015**, *44*, 5148-5180.
(2) Schrauzer, G. N.; Guth, T. D. Photocatalytic Reactions. 1. Photolysis of Water and Photoreduction of Nitrogen on Titanium Dioxide. *J. Am. Chem. Soc.* **1977**, *99*, 7189-7193.
(3) Schrauzer, G. N.; Guth, T. D. Photolysis of Water and Photoreduction of Nitrogen on Titanium-Dioxide. *J. Am. Chem. Soc.* **1977**, *99*, 7189-7193.

(4) Fujishima, A.; Honda, K. Electrochemical Photolysis of Water at a Semiconductor Electrode. *Nature* **1972**, *238*, 37.

(5) Dahl, M.; Liu, Y.; Yin, Y. Composite Titanium Dioxide Nanomaterials. *Chem. Rev.* **2014**, *114*, 9853-9889.

(6) Shi, L.; Li, Z.; Dao, T. D.; Nagao, T.; Yang, Y. A Synergistic Interaction between Isolated Au Nanoparticles and Oxygen Vacancies in an Amorphous Black TiO2 Nanoporous Film: toward Enhanced Photoelectrochemical Water Splitting. *J. Mater. Chem. A* **2018**, *6*, 12978-12984.

(7) Li, Z.; Shi, L.; Franklin, D.; Koul, S.; Kushima, A.; Yang, Y. Drastic Enhancement of Photoelectrochemical Water Splitting Performance over Plasmonic Al@TiO2 Heterostructured Nanocavity Arrays. *Nano Energy* **2018**, *51*, 400-407.

(8) Schneider, J.; Matsuoka, M.; Takeuchi, M.; Zhang, J.; Horiuchi, Y.; Anpo, M.; Bahnemann, D. W. Understanding TiO_2 Photocatalysis: Mechanisms and Materials. *Chem. Rev.* **2014**, *114*, 9919-9986.

(9) Carp, O.; Huisman, C. L.; Reller, A. Photoinduced Reactivity of Titanium Dioxide. *Prog. Solid State Chem.* **2004**, *32*, 33-177.

(10) Bickley, R. I.; Gonzalez-Carreno, T.; Lees, J. S.; Palmisano, L.; Tilley, R. J. D. A Structural Investigation of Titanium Dioxide Photocatalysts. *J. Solid State Chem.* **1991**, *92*, 178-190.

(11) Kho, Y. K.; Iwase, A.; Teoh, W. Y.; Mädler, L.; Kudo, A.; Amal, R. Photocatalytic H_2 Evolution over TiO_2 Nanoparticles. The Synergistic Effect of Anatase and Rutile. *J. Phys. Chem. C* **2010**, *114*, 2821-2829.

(12) Li, G.; Richter, C. P.; Milot, R. L.; Cai, L.; Schmuttenmaer, C. A.; Crabtree, R. H.; Brudvig, G. W.; Batista, V. S. Synergistic Effect between Anatase and Rutile TiO_2 Nanoparticles in Dye-Sensitized Solar Cells. *Dalton Trans.* **2009**, 10078-10085.

(13) Ohtani, B.; Prieto-Mahaney, O. O.; Li, D.; Abe, R. What is Degussa (Evonik) P25? Crystalline Composition Analysis, Reconstruction from Isolated Pure Particles and Photocatalytic Activity Test. *J. Photochem. Photobiol. A* **2010**, *216*, 179-182.

(14) Nosaka, Y.; Nosaka, A. Y. Reconsideration of Intrinsic Band Alignments within Anatase and Rutile TiO_2. *J. Phys. Chem. Lett.* **2016**, *7*, 431-434.

(15) Scanlon, D. O.; Dunnill, C. W.; Buckeridge, J.; Shevlin, S. A.; Logsdail, A. J.; Woodley, S. M.; Catlow, C. R. A.; Powell, M. J.; Palgrave, R. G.; Parkin, I. P.; Watson, G. W.; Keal, T. W.; Sherwood, P.; Walsh, A.; Sokol, A. A. Band alignment of Rutile and Anatase TiO_2. *Nat. Mater.* **2013**, *12*, 798.

(16) Su, R.; Bechstein, R.; Sø, L.; Vang, R. T.; Sillassen, M.; Esbjörnsson, B.; Palmqvist, A.; Besenbacher, F. How the Anatase-to-Rutile Ratio Influences the Photoreactivity of TiO_2. *J. Phys. Chem. C* **2011**, *115*, 24287-24292.

(17) Sun, B.; Smirniotis, P. G. Interaction of Anatase and Rutile TiO_2 Particles in Aqueous Photooxidation. *Catal. Today* **2003**, *88*, 49-59.

(18) Malekshahi Byranvand, M.; Nemati Kharat, A.; Fatholahi, L.; Malekshahi Beiranvand, Z. A Review on Synthesis of Nano-TiO_2 via Different Methods. *J. Nanostruct.* **2013**, *3*, 1-9.

(19) Valizadeh, B.; Nguyen, T. N.; Stylianou, K. C. Shape Engineering of Metal–Organic Frameworks. *Polyhedron* **2018**, *145*, 1-15.

(20) Bin, L.; Hui-Min, W.; Yuanjing, C.; Wei, Z.; Guodong, Q.; Banglin, C. Emerging Multifunctional Metal–Organic Framework Materials. *Adv. Mater.* **2016**, *28*, 8819-8860.

(21) Li, L.; Li, X.; Ai, L.; Jiang, J. MOF-Derived Nanostructured Cobalt Phosphide Assemblies for Efficient Hydrogen Evolution Reaction. *RSC Adv.* **2015**, *5*, 90265-90271.

(22) Jagadeesh, R. V.; Murugesan, K.; Alshammari, A. S.; Neumann, H.; Pohl, M.-M.; Radnik, J.; Beller, M. MOF-Derived Cobalt Nanoparticles Catalyze a General Synthesis of Amines. *Science* **2017**, *358*, 326–332.

(23) Rui, W.; Xi-Yan, D.; Jiao, D.; Jin-Yan, Z.; Shuang-Quan, Z. MOF-Derived Bifunctional Cu_3P Nanoparticles Coated by a N,P-Codoped Carbon Shell for Hydrogen Evolution and Oxygen Reduction. *Adv. Mater.* **2018**, *30*, 1703711.

(24) Kumar, D. P.; Choi, J.; Hong, S.; Reddy, D. A.; Lee, S.; Kim, T. K. Rational Synthesis of Metal–Organic Framework-Derived Noble Metal-Free Nickel Phosphide Nanoparticles as a Highly Efficient Cocatalyst for Photocatalytic Hydrogen Evolution. *ACS Sustain. Chem. Eng.* **2016**, *4*, 7158-7166.

(25) Tian, T.; Ai, L.; Jiang, J. Metal–Organic Framework-derived Nickel Phosphides as Efficient Electrocatalysts toward Sustainable Hydrogen Generation from Water Splitting. *RSC Adv.* **2015**, *5*, 10290-10295.

(26) Xiu, Z.; Alfaruqi, M. H.; Gim, J.; Song, J.; Kim, S.; Thi, T. V.; Duong, P. T.; Baboo, J. P.; Mathew, V.; Kim, J. Hierarchical Porous Anatase TiO_2 Derived from a Titanium Metal–Organic Framework as a Superior Anode Material for Lithium Ion Batteries. *Chem. Commun.* **2015**, *51*, 12274-12277.

(27) Oar-Arteta, L.; Wezendonk, T.; Sun, X.; Kapteijn, F.; Gascon, J. Metal Organic Frameworks as Precursors for the Manufacture of Advanced Catalytic Materials. *Mater. Chem. Front.* **2017**, *1*, 1709-1745.

(28) Zhao, S.-N.; Song, X.-Z.; Song, S.-Y.; Zhang, H.-j. Highly Efficient Heterogeneous Catalytic Materials Derived from Metal-Organic Framework Supports/Precursors. *Coord. Chem. Rev.* **2017**, *337*, 80-96.

(29) Bhadra, B. N.; Song, J. Y.; Khan, N. A.; Jhung, S. H. TiO_2-Containing Carbon Derived from a Metal–Organic Framework Composite: A Highly Active Catalyst for Oxidative Desulfurization. *ACS Appl. Mater. Interfaces* **2017**, *9*, 31192-31202.

(30) Dan-Hardi, M.; Serre, C.; Frot, T.; Rozes, L.; Maurin, G.; Sanchez, C.; Férey, G. A New Photoactive Crystalline Highly Porous Titanium(IV) Dicarboxylate. *J. Am. Chem. Soc.* **2009**, *131*, 10857-10859.

(31) Hu, S.; Liu, M.; Li, K.; Zuo, Y.; Zhang, A.; Song, C.; Zhang, G.; Guo, X. Solvothermal Synthesis of NH_2-MIL-125(Ti) from Circular Plate to Octahedron. *Cryst. Eng. Comm.* **2014**, *16*, 9645-9650.

(32) Nguyen, T. N.; Kampouri, S.; Valizadeh, B.; Luo, W.; Ongari, D.; Planes, O. M.; Züttel, A.; Smit, B.; Stylianou, K. C. Photocatalytic Hydrogen Generation from a Visible-Light-Responsive Metal–Organic Framework System: Stability versus Activity of Molybdenum Sulfide Cocatalysts. *ACS Appl. Mater. Interfaces* **2018**, *10*, 30035-30039.

(33) Khaletskaya, K.; Pougin, A.; Medishetty, R.; Rösler, C.; Wiktor, C.; Strunk, J.; Fischer, R. A. Fabrication of Gold/Titania Photocatalyst for CO_2 Reduction Based on Pyrolytic Conversion of the Metal–Organic Framework NH_2-MIL-125(Ti) Loaded with Gold Nanoparticles. *Chem. Mater.* **2015**, *27*, 7248-7257.

(34) Yan, B.; Zhang, L.; Tang, Z.; Al-Mamun, M.; Zhao, H.; Su, X. Palladium-Decorated Hierarchical Titania Constructed from the Metal-Organic Frameworks NH_2-MIL-125(Ti) as a Robust Photocatalyst for Hydrogen Evolution. *Appl. Catal., B* **2017**, *218*, 743-750.

(35) Kampouri, S.; Nguyen, T. N.; Ireland, C. P.; Valizadeh, B.; Ebrahim, F. M.; Capano, G.; Ongari, D.; Mace, A.; Guijarro, N.; Sivula, K.; Sienkiewicz, A.; Forro, L.; Smit, B.; Stylianou, K. C. Photocatalytic Hydrogen Generation from a Visible-Light Responsive Metal-Organic Framework System: The Impact of Nickel Phosphide Nanoparticles. *J. Mater. Chem. A* **2018**, *6*, 2476-2481.

(36) Hanaor, D. A. H.; Sorrell, C. C. Review of the Anatase to Rutile Phase Transformation. *J. Mater. Sci.* **2011**, *46*, 855-874.

(37) Particle Size Effects on Transformation Kinetics and Phase Stability in Nanocrystalline TiO_2. *Am. Mineral.* **1997**, *82*, 717-728.

(38) Zhang, Z.; Brown, S.; Goodall, J. B. M.; Weng, X.; Thompson, K.; Gong, K.; Kellici, S.; Clark, R. J. H.; Evans, J. R. G.; Darr, J. A. Direct Continuous Hydrothermal Synthesis of High Surface Area Nanosized Titania. *J. Alloys Compd.* **2009**, *476*, 451-456.

(39) Kapilashrami, M.; Zhang, Y.; Liu, Y.-S.; Hagfeldt, A.; Guo, J. Probing the Optical Property and Electronic Structure of TiO_2 Nanomaterials for Renewable Energy Applications. *Chem. Rev.* **2014**, *114*, 9662-9707.

(40) Ohno, T.; Sarukawa, K.; Tokieda, K.; Matsumura, M. Morphology of a TiO_2 Photocatalyst (Degussa, P-25) Consisting of Anatase and Rutile Crystalline Phases. *J. Catal.* **2001**, *203*, 82-86.

(41) Assi, H.; Pardo Pérez, L. C.; Mouchaham, G.; Ragon, F.; Nasalevich, M.; Guillou, N.; Martineau, C.; Chevreau, H.; Kapteijn, F.; Gascon, J.; Fertey, P.; Elkaim, E.; Serre, C.; Devic, T. Investigating the Case of Titanium(IV) Carboxyphenolate Photoactive Coordination Polymers. *Inorg. Chem.* **2016**, *55*, 7192-7199.

(42) Qureshi, M.; Takanabe, K. Insights on Measuring and Reporting Heterogeneous Photocatalysis: Efficiency Definitions and Setup Examples. *Chem. Mater.* **2017**, *29*, 158-167.

(43) Emeline, A. V.; Ryabchuk, V. K.; Serpone, N. Dogmas and Misconceptions in Heterogeneous Photocatalysis. Some Enlightened Reflections. *J. Phys. Chem. B* **2005**, *109*, 18515-18521.

TOC: